Journal of Naval Architecture and Marine Engineering
January, 2026
https://dx.doi.org/10.3329/jname.v23i1.76997 *https://www.banglajol.info*

MHD PULSATILE FLOW OF JEFFREY LIQUID LAYERS SEPARATED BY MICROPOLAR LIQUID LAYER BETWEEN PERMEABLE BEDS

V. Madhurya[1*] and S. Srinivas[2]
Department of Mathematics, VIT-AP University, Inavolu, Amaravathi-522237, India
[1*]madhurya6699@gmail.com, [2]srinusuripeddi@hotmail.com

Abstract:

This study explores the magnetohydrodynamic (MHD) pulsatile flow of Jeffrey liquid layers separated by a micropolar liquid layer, confined between two permeable beds. The flow domain is divided into three distinct regions: Regions A and C, which contain Jeffrey fluid, and Region B, which contains a micropolar fluid. The liquid - permeable bed interfaces are governed by the Beavers–Joseph slip boundary condition. The governing equations are solved numerically using the NDSolve function in Mathematica. The effects of various physical parameters on velocity profiles, mass flux, and microrotation velocity are illustrated graphically. Additionally, stress distributions are analyzed and presented in tabular form. The results reveal that the applied magnetic field has a pronounced influence on the flow characteristics compared to the purely hydrodynamic case. Our analysis indicates that the stress distribution at the permeable boundaries increases with Reynolds number, slip coefficient, porosity, and Jeffrey fluid parameters. Furthermore, mass flux is found to increase with the Reynolds number, Jeffrey parameter, and micropolar material parameter, while it decreases with an increase in the Hartmann number. A comparative analysis of our results with other researchers shows good agreement.

Keywords: *Permeable bed, pulsating flow, Jeffrey fluid, microrotation parameter, magnetic field.*

NOMENCLATURE

t	Time
Q	Instantaneous mass flux
C_p	Coupling parameter
P_j	Microrotation parameter
n	Gyration parameter
m	Micropolar material parameter
k	Vortex viscosity of micropolar
c	Microrotation velocity
p	Pressure
B_0	Applied magnetic field strength
$\overline{J}$	Electric current density
j	Microinertia density
$\overline{q}$	Velocity vector
$\overline{v}$	Microrotation vector
$\overline{B}$	Total magnetic field
$\overline{f},\overline{l}$	Body force and body couple
x, y	axial and transverse coordinates
K_1, K_2	Permeability of porous beds
Q_1, Q_2	Darcy velocities at permeable beds
u_1, u_2, u_3	Velocity components of Region A, B, C

Greek symbols

τ	Shear stress
ω	Frequency parameter
α	Slip parameter
δ	Interface height
δ_1	Dimensionless interface height
α_1, β, γ	Micro viscosity coefficients
ρ, ρ'	Ratio of viscosity
σ_1, σ_2	Permeability parameters
λ_1, λ_2	Jeffrey parameters
μ, μ'	Ratio of density
$\sigma_{*1}, \sigma_{*2}, \sigma_{*3}$	Electrical conductivity
μ_1, μ_2, μ_3	Dynamic viscosity
ρ_1, ρ_2, ρ_3	Fluid density

Subscripts

1 — Region A (Jeffrey fluid)
2 — Region B (Micropolar fluid)
3 — Region C (Jeffrey fluid)
s— Steady component
o— Oscillatory component

Abbreviations

1813-8535 (Print), 2070-8998 (Online) Received: Oct., 2024

M_1, M_2, M_3	Hartmann numbers	UPB	— Upper Permeable Bed
R_1, R_2, R_3	Reynolds numbers	LPB	— Lower Permeable Bed

1. Introduction

Pulsating flows are frequently seen in various engineering applications that deal with the dynamics of liquids. Pulsating flows have diverse applications, including the pumping of mixtures containing both solids and liquids, mitigating cavitation in hydraulic systems Chaudhry (2014), pressure surges in pipelines, and more. Several technological disciplines that utilise pulsatile flows include cardiovascular biomechanics, combustion systems, and refrigeration technology. The reader can find a comprehensive treatise on this topic by Zamir et al. (2002). Many researchers have extensively studied pulsatile flow problems involving Newtonian and non-Newtonian liquids in various flow scenarios (Chaudhry, 2014; Zamir et al., 2002; Wang, 1971; Valueva and Purdin, 2015; Bhattacharya and Nanda, 1979; Sankar and Lee, 2009; Selvi and Muthuraj, 2018; Ali et al., 2020; Kim et al., 1994; Rajkumar et al., 2025; Okedoye, 2025). Wang (1971) performed an analytical investigation on the pulsatile flow through a porous channel. Analytical expressions for velocity and the mass flux have derived, in his study, under the assumption that a fluid is injected into one plate with a certain velocity and then extracted from the opposite plate at the same velocity. Valueva and Purdin (2015) conducted a numerical investigation on the pulsating laminar flow in a rectangular channel. Equations that represent the flow were solved by employing the finite difference method. The impact of the aspect ratio of the sides of a rectangular channel on the dynamics of pulsating flow has been examined. Bhattacharya and Nanda (1979) conducted analytical research on the pulsatile flow of a viscous fluid in a rotating channel and obtained an exact solution for the flow. The impact of Ekmann number and frequency parameters on important flow characteristics, such as the average sectional velocity and shear forces on the plates have been examined. Sankar and Lee (2009) proposed a mathematical model for pulsatile flow of non-Newtonian fluid in narrowed arteries. The authors employed the perturbation approach to investigate the flow and obtained an analytical solution for the velocity, longitudinal impedance, plug core radius, flow rate, and shear stress. Selvi and Muthuraj (2018) analysed the oscillatory flow of a Jeffrey fluid with magnetohydrodynamics and viscosity dissipation in a vertical channel. The outcome of the study reveals that fluid temperature increases with thermal parameters, Brinkmann number and Dufour number, while decreasing with inertia coefficient. Ali et al. (2020) conducted a numerical investigation on the pulsating flow of a micropolar-Casson fluid in a channel in a Darcian porous material with a magnetic field. The study indicates that the wall shear stress (WSS) increases when the values of the Hartman, Casson, and micropolar liquid parameters increase, and WSS falls with a rise in the porosity parameter. The flow separation regime is demonstrated to be significantly affected by the Hartman number. Kim et al. (1994) conducted a study on the heat transfer characteristics of forced pulsating flow in a channel filled with fluid-saturated porous media. The authors used Finite-volume methods to solve time-dependent, two-dimensional Darcy model equations and found that, with the increase in pulsation frequency, the Nusselt number reaches its maximum at more upstream positions. Their results indicate that the Nusselt number at the upper wall rises as the heat source increases, and it falls as the radiation parameter increases. However, this behaviour is inverted at the bottom wall. Rajkumar et al. (2025) examined the impact of Cattaneo-Christov heat flux and Buongiorno nanofluid model on entropy generation in pulsating hydromagnetic flow of a micropolar nanofluid in a porous channel. The outcome of the study reveals that, by increasing viscous dissipation, Brownian motion, and thermal radiation parameters leads to the entropy generation enhancement.

Immiscible fluid flow is crucial in oil recovery, environmental management, and chemical processes. It helps in enhanced oil extraction, managing spills, and separating components in chemical engineering. Its principles are also applied in pharmaceuticals, food processing, and microfluidics. Furthermore, it plays a vital role in creating sophisticated mathematical and computational models as well as for biological applications like blood flow analysis. Several authors have extensively investigated immiscible pulsatile flow problems with Newtonian and non-Newtonian liquids in different flow conditions (Chamkha et al., 2004; Allan et al., 2008; Umavathi et al., 2014; Umavathi and Hemavathi, 2018; Padma and Srinivas, 2023; Padma et al., 2024; Komal and Srinivas, 2024a; Komal and Srinivas, 2024b). Chamkha et al. (2004) explored oscillatory flow and heat transfer in two immiscible fluids and their findings indicate that, with the rise of the viscosity ratio the velocity distribution decreases. Furthermore, there is a fall in temperature distribution. Padma and Srinivas (2023) examined the combined impact of Hall current, thermal radiation, heat source, and chemical reaction on the heat and mass characteristics in a vertical porous channel filled with a two-layered viscoelastic liquid. Allan et al. (2008) conducted a study on characteristics of liquid flow through three porous layers, and their analysis shows that the velocity at interfaces does not significantly change, in spite of the difference in the Darcy numbers of the upper and lower regions. The heat transfer effects of two micropolar liquid layers separated by a viscous fluid layer in a three-layer fluid flow

model are reported by Umavathi et al. (2014). It is reported that as the rise of the conductivity ratio increases, the temperature distribution becomes suppressed in the vicinity of the lower plate, whereas it enhances in the vicinity of the upper plate. Recently, Padma et al. (2024) numerically investigated the unsteady two-immiscible MHD free convective flow of Casson liquid through a vertical channel with a porous medium. Their observation indicates that in both slip and no-slip scenarios, entropy production decreases as the magnetic field intensity increases. In a more recent study, Komal and Srinivas (2024a) conducted a study on MHD two-layered pulsatile flow in a corrugated curved channel. Their study unveiled that, at the outer channel wall, stress reduces as the frequency parameter increases, but it shows a reverse tendency at the lower channel wall. The flow of a three-layered immiscible fluid in a permeable inclined channel subjected to a pulsatile pressure gradient was studied by Komal and Srinivas (2024b). Their findings reveal that lamina-shaped nanoparticles shows the highest rate of heat transfer. Further, the Sherwood number fluctuates with time and is lower at the upper boundary of the channel compared to the lower boundary.

Recent advances in research have concentrated on fluid dynamics in porous media (Chandrapushpam et al., 2023; Bhuvaneswari and Sivasankaran, 2024; Hakeem et al., 2024; and Sivanandam and Turki, 2025) highlighting the role of porous structures in facilitating complex flow dynamics and energy transport. Permeable beds, which are a specific form of porous media, play a vital role for effective water infiltration, groundwater recharge, and stormwater management, which are widely used in environmental engineering, civil infrastructure, and flood control systems to enhance drainage and reduce runoff, Many researchers have investigated pulsatile flow problems involving Newtonian and non-Newtonian liquids between permeable beds (Vajravelu et al., 1995; Malathy and Srinivas, 2008; Iyengar and Bitla, 2011; Bitla and Iyengar, 2013; Bitla and Iyengar, 2014; kumar and Agarwal, 2021; Mukherjee and Shit, 2022) . A numerical investigation on unsteady immiscible conducting fluids between permeable beds was conducted by Vajravelu et al. (1995). Malathy and Srinivas (2008) have reported the pulsating flow of a hydromagnetic fluid between two permeable beds. In their model, they have assumed that the liquid is injected at a velocity through the bottom permeable bed and then drawn out of the channel with the same velocity from the upper permeable bed. The volume flux and velocity expressions were derived analytically under the assumption that the Navier-Stokes equation governs the flow between beds and Darcy's law regulates the flow through the porous beds. Iyengar and Bitla (2011) have explored pulsating movement of an incompressible couple-stress fluid between permeable beds, and they observed that as the porosity parameter rises, both the velocity and the unsteady velocity component diminish. Moreover, the stress distribution at both walls decreases with increasing porosity for $\omega t = \pi/4$ and $\pi/2$ and it increases for $\omega t = 0$ and $3\pi/4$. In a separate study, Bitla and Iyengar (2014) explored the pulsating flow of an incompressible, mildly conducting micropolar fluid between two uniform permeable beds with an inclined magnetic field, and they found that increasing the magnetic field's inclination angle enhances the velocity. Additionally, asymmetry in microrotation is observed in the flow region, where it aligns with a plane closer to and parallel to the upper bed. microrotation exhibits asymmetry in the flow region, aligning with a plane nearer to and parallel to the upper bed. The problem of MHD pulsating flow and heat transfer effects of two immiscible, incompressible conducting couple-stress liquids between permeable beds has been modelled by Kumar and Agarwal (2021). Their work demonstrates that the stress distribution at both permeable beds rises with increasing density ratio, slip, Reynolds number, and couple stress parameters, but decreases with increasing viscosity ratio. Further, there is a rise in the velocity and temperature distributions of the liquid with the rise of the slip parameter, while an opposite behaviour is noticed with an increase in the porosity parameter. Mukherjee and Shit (2022) analysed the impact of the ion diffusion coefficient on the problem of constant electroosmotic couple stress in nanofluid flow and heat transfer within a porous microchannel that is enclosed by two permeable beds. Their results highlighted that nanofluid temperature enhances with a rise in the couple stress parameter and porous permeability, but decreases as the ion diffusion coefficient falls.

Although numerous investigations have been conducted on flows between permeable beds, information regarding immiscible flows between them remains limited. Motivated by previous studies, a mathematical model related to immiscible flow between permeable beds is presented as such an investigation is not yet been reported in the literature. These studies are crucial in various fields, including hydrology, chemical processes, biomedical systems, and petroleum engineering. Non-Newtonian fluids, such as micropolar and Jeffrey liquids, are essential in biomedical, industrial, and material processing applications for accurately modelling the complex behaviours of suspensions and emulsions. The key objective of this research is to develop a mathematical model and address the problem of a three-layer magnetohydrodynamic pulsating flow between permeable beds with periodic pressure gradient. The proposed model divides the flow between permeable beds into three distinct regions: Regions A and C, which are filled with Jeffrey liquid, and Region B, which contains a micropolar liquid. The interfaces

between the permeable beds are governed by the Beavers-Joseph slip boundary conditions. The governing flow equations are numerically solved with NDSolve command of Mathematica package and the role of pertinent parameters on velocity, mass flux and microrotation velocity have been shown graphically. Furthermore, results for stress distribution are presented in tabular form and analyzed.

2. Mathematical Formulation

This work examines the flow in a channel between two permeable beds of indefinite length in the x direction, with the y axis separated by a distance h and δ. Figure 1 illustrates the partitioning of the channel into three separate sections, denoted as regions A, B, and C. Region A $(-h \le y \le 0)$ filled with Jeffrey liquid with density ρ_1 and viscosity μ_1. Region B $(0 \le y \le \delta)$ filled with micropolar liquid with a density of ρ_2 and the viscosity of μ_2 and Region C filled with Jeffrey liquid occupy the space $(\delta \le y \le 2h)$ with density ρ_3 and viscosity μ_3.

The field equations of micropolar fluid Eringen (1966, 2001) are

$$\left.\begin{aligned} &\frac{\partial \rho}{\partial t} + \nabla.\left(\rho \bar{q}\right) = 0. \\ &\rho \frac{d\bar{q}}{dt} = \rho \bar{f} - \nabla p + k\nabla \times \bar{\upsilon} - \left(\mu + k\right)\left(\nabla \times \nabla \times \bar{q}\right) + \left(\lambda + 2\mu + k\right)\nabla\left(\nabla.\bar{q}\right) + \bar{J} \times \bar{B} \\ &\rho j \frac{d\bar{\upsilon}}{dt} = \rho \bar{l} - 2k\bar{\upsilon} + k\nabla \times \bar{q} - \gamma\left(\nabla \times \nabla \times \bar{\upsilon}\right) + \left(3\alpha_1 + \beta + \gamma\right)\nabla\left(\nabla.\bar{\upsilon}\right) \end{aligned}\right\} \quad (1)$$

Where $\bar{q}$ and $\bar{\upsilon}$ for velocity and microrotation vectors respectively. The variables $\bar{f}$ and $\bar{l}$ represent the body force and body couple per unit mass, respectively while p, ρ, j, J, represents the pressure at any point, fluid density, microinertia density, and current density, in that order and B denotes total magnetic field, which is the combined value of the applied and induced magnetic fields. The conditions that material quantities (λ_*, μ, k) and the micro-viscosity coefficients $(\alpha_1, \beta, \gamma)$ satisfy are presented in Bitla and Iyengar (2013).

The field equations of the Jeffrey fluid are

$$\left.\begin{aligned} &\nabla.\bar{q} = 0 \\ &\rho \frac{d\bar{q}}{dt} = -\nabla p + \bar{J} \times \bar{B} + \mu\left(\frac{1}{1+\lambda}\right)\nabla^2 \bar{q} \end{aligned}\right\} \quad (2)$$

This analysis is carried out based on the following assumptions. i) The fluids are non-compressible and immiscible. ii) The permeable beds are rigid and homogeneous. iii) The flow is fully developed and laminar. iv) The fluid motion is driven by an unsteady pressure gradient $-\frac{\partial p}{\partial x} = \left(\frac{\partial p}{\partial x}\right)_s + \left(\frac{\partial p}{\partial x}\right)_o e^{i\omega t}$, where ω is the frequency, $\left(\frac{\partial p}{\partial x}\right)_o$ and $\left(\frac{\partial p}{\partial x}\right)_s$ are the amplitudes of oscillatory and steady pulsations, respectively.

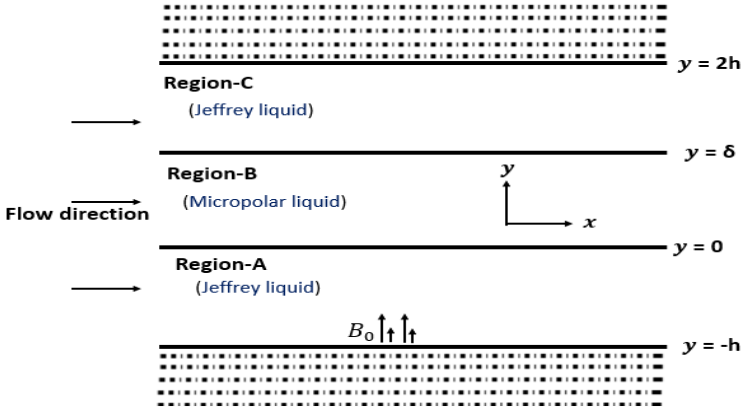

Fig. 1: Schematic flow

Under the assumptions we made for region-B, $\bar{q}$ as $(\bar{u}(y,t),0,0)$ and $\bar{\upsilon}$ as $(0,0,c(y,t))$ and for Region-A, C $\bar{q}$ as $(\bar{u}(y,t),0,0)$.

The governing flow equations, when no body forces and couples present, are:

Region – A

$$\rho_1 \frac{\partial u_1}{\partial t} = -\frac{\partial P}{\partial x} + \frac{\mu_1}{1+\lambda_1}\frac{\partial^2 u_1}{\partial y^2} - \sigma_{*1} {B_0}^2 u_1. \tag{3}$$

Region - B

$$\begin{aligned} \rho_2 \frac{\partial u_2}{\partial t} &= -\frac{\partial P}{\partial x} + (\mu_2 + k)\frac{\partial^2 u_2}{\partial y^2} + k\frac{\partial c}{\partial y} - \sigma_{*2} {B_0}^2 u_2 \\ \rho_2 j \frac{\partial c}{\partial t} &= -2kc - k\frac{\partial u_2}{\partial y} + \gamma \frac{\partial^2 c}{\partial y^2}. \end{aligned} \tag{4}$$

Region – C

$$\rho_3 \frac{\partial u_3}{\partial t} = -\frac{\partial P}{\partial x} + \frac{\mu_3}{1+\lambda_2}\frac{\partial^2 u_3}{\partial y^2} - \sigma_{*3} {B_0}^2 u_3. \tag{5}$$

The velocity component $u(y,t)$ and the microrotation component c(y, t) must adhere to the specified boundary conditions.

$$\frac{\partial u_1}{\partial y} = \frac{\alpha}{\sqrt{K_1}}\left(u_1' - Q_1\right), u_1' = u_1 \qquad \text{at} \quad y = -h \tag{6}$$

$$\frac{\mu_1}{1+\lambda_1}\frac{\partial u_1}{\partial y} = (\mu_2 + k)\frac{\partial u_2}{\partial y} + kc, c = 0, u_1 = u_2 \qquad \text{at} \quad y = 0 \tag{7}$$

$$\frac{\mu_3}{1+\lambda_2}\frac{\partial u_3}{\partial y} = (\mu_2 + k)\frac{\partial u_2}{\partial y} + kc, c = 0, u_2 = u_3 \qquad \text{at} \quad y = \delta \tag{8}$$

$$\frac{\partial u_3}{\partial y} = -\frac{\alpha}{\sqrt{K_2}}\left(u_3' - Q_2\right), u_3' = u_3 \qquad \text{at} \quad y = 2h \tag{9}$$

At the interfaces $y = 0$ and $y = \delta$ microrotation velocity $c(y,t)$ vanishes and at the $y = -h$ and $y = 2h$ boundary conditions of B-J slip Beavers and Joseph (1967) are considered. For the upper permeable bed(UPB), $Q_1 = -\frac{K_1}{\mu_1}\frac{\partial p}{\partial x}$ describes the Darcy velocity, and for lower permeable bed(LPB), it is given $Q_2 = -\frac{K_2}{\mu_3}\frac{\partial p}{\partial x}$. The slip velocities at their respective interfaces of beds are u_1' and u_3'.

$$u_j = u_{j1} + u_{j2} e^{i\omega t}, \ (j = 1,2,3), \quad c = c_s + c_o e^{i\omega t} \tag{10}$$

where the steady parts of the velocity and microrotation are denoted by u_{j1} and c_s, and the oscillatory parts by u_{j2} and c_o, respectively.

2.1 Non-dimensional flow quantities

The following dimensionless variables are defined to convert governing equations and boundary conditions into a dimensionless form:

$$\begin{aligned} &x^* = \frac{x}{h}, y^* = \frac{y}{h}, u_j^* = \frac{u_j}{u}, u_{j1}^* = \frac{u_{j1}}{u}, u_{j2}^* = \frac{u_{j2}}{u}, c^* = \frac{ch}{u}, \\ &c_s^* = \frac{c_s h}{u}, c_o^* = \frac{c_o h}{u}, t^* = \frac{tu}{h}, \omega^* = \frac{\omega h}{u}, p^* = \frac{p}{\rho u^2}, \delta_1 = \frac{\delta}{h}. \end{aligned} \tag{11}$$

After dropping the asterisks, the flow equations and boundary conditions (3-9) provided by

$$\frac{\partial u_1}{\partial t} = -\frac{\partial P}{\partial x} + \frac{1}{R_1(1+\lambda_1)}\frac{\partial^2 u_1}{\partial y^2} - \frac{{M_1}^2}{R_1} u_1 \tag{12}$$

$$\frac{\partial u_2}{\partial t} = -\rho\frac{\partial P}{\partial x} + \frac{1}{R_2}\frac{\partial^2 u_2}{\partial y^2} + \frac{C_p}{R_2}\frac{\partial c}{\partial y} - \frac{{M_2}^2}{R_2}u_2$$
$$\frac{\partial c}{\partial t} = -\frac{2n}{R_2 P_j}c - \frac{n}{R_2 P_j}\frac{\partial u_2}{\partial y} + \frac{1}{R_2 P_j}\frac{\partial^2 c}{\partial y^2} \quad (13)$$

$$\frac{\partial u_3}{\partial t} = -\rho'\frac{\partial P}{\partial x} + \frac{1}{R_3(1+\lambda_2)}\frac{\partial^2 u_3}{\partial y^2} - \frac{{M_3}^2}{R_3}u_3 \quad (14)$$

$$\frac{\partial u_1}{\partial y} = \alpha\sigma_1\left(u_1' + \frac{R_1}{{\sigma_1}^2}\frac{\partial p}{\partial x}\right),\ u_1' = u_1 \qquad \text{at} \quad y = -1 \quad (15)$$

$$\frac{\mu}{m(1+\lambda_1)}\frac{\partial u_1}{\partial y} = \frac{1}{C_p}\frac{\partial u_2}{\partial y} + c,\ c = 0,\ u_1 = u_2 \qquad \text{at} \quad y = 0 \quad (16)$$

$$\frac{\mu'}{m(1+\lambda_2)}\frac{\partial u_3}{\partial y} = \frac{1}{C_p}\frac{\partial u_2}{\partial y} + c, c = 0, u_2 = u_3 \qquad \text{at} \quad y = \delta_1 \quad (17)$$

$$\frac{\partial u_3}{\partial y} = -\alpha\sigma_2\left(u_3' + \rho'\frac{R_3}{{\sigma_2}^2}\frac{\partial p}{\partial x}\right),\ u_3' = u_3 \qquad \text{at} \quad y = 2 \quad (18)$$

Here, $M_1 = B_0 h\sqrt{\frac{\sigma_{*1}}{\rho_1 \upsilon_1}}$ $M_2 = B_0 h\sqrt{\frac{\sigma_{*2}}{\mu_2 + k}}$, $M_3 = B_0 h\sqrt{\frac{\sigma_{*3}}{\rho_3 \upsilon_3}}$, $R_1 = \frac{\rho_1 uh}{\mu_1}$, $R_2 = \frac{\rho_2 uh}{\mu_2 + k}$, $R_3 = \frac{\rho_3 uh}{\mu_3}$, the variables M_1, M_2, M_3 represent the Hartmann numbers for Regions A, B, and C, respectively, while R_1, R_2, R_3 denotes the corresponding Reynolds numbers for these Regions. $\sigma_1 = h/\sqrt{K_1}$, $\sigma_2 = h/\sqrt{K_2}$ are non-dimensional characteristics that have an inverse relationship with the square root of the permeabilities in regions A and C. $C_p = \frac{k}{\mu_2 + k}$, $P_j = \frac{j(\mu_2 + k)}{\gamma}$, $n = \frac{kh^2}{\gamma}$, $m = \frac{k}{\mu_2}$, B_0, α, σ_{*j} represent Coupling, microrotation, gyration, micropolar liquid material parameters, external magnetic field, Slip parameter, and thermal conductivity respectively. $\rho = \frac{\rho_1}{\rho_2}$, $\rho' = \frac{\rho_1}{\rho_3}$, $\mu = \frac{\mu_1}{\mu_2}$ and $\mu' = \frac{\mu_3}{\mu_2}$ are ratios of density and viscosity, and λ_1, λ_2 are Jeffrey liquid parameters for Region-A and C.

The steady flow equations and boundary conditions are:

$$\frac{d^2 u_{11}}{dy^2} - {M_1}^2(1+\lambda_1)u_{11} + R_1(1+\lambda_1)P_s = 0 \quad (19)$$

$$\frac{d^2 u_{21}}{dy^2} + C_p\frac{dc_s}{dy} - {M_2}^2 u_{21} + \rho R_2 P_s = 0$$
$$\frac{d^2 c_s}{dy^2} - n\frac{du_{21}}{dy} - 2nc_s = 0. \quad (20)$$

$$\frac{d^2 u_{31}}{dy^2} - {M_3}^2(1+\lambda_2)u_{31} + \rho' R_3(1+\lambda_2)P_s = 0 \quad (21)$$

$$\frac{\partial u_{11}}{\partial y} = \alpha\sigma_1\left(u_{11}' - \frac{R_1}{{\sigma_1}^2}P_s\right), u_{11}' = u_{11} \qquad \text{at} \quad y = -1 \quad (22)$$

$$\frac{\mu}{m(1+\lambda_1)}\frac{\partial u_{11}}{\partial y} = \frac{1}{C_p}\frac{\partial u_{21}}{\partial y} + c_s, c_s = 0, u_{11} = u_{21} \qquad \text{at} \quad y = 0 \quad (23)$$

$$\frac{\mu'}{m(1+\lambda_2)}\frac{\partial u_{31}}{\partial y} = \frac{1}{C_p}\frac{\partial u_{21}}{\partial y} + c_s, c_s = 0, u_{21} = u_{31} \qquad \text{at} \quad y = \delta_1 \quad (24)$$

$$\frac{\partial u_{31}}{\partial y} = -\alpha\sigma_2\left(u_{31}' - \rho'\frac{R_3}{{\sigma_2}^2}P_s\right), u_{31}' = u_{31} \qquad \text{at} \quad y = 2 \quad (25)$$

The Oscillatory flow equations and boundary conditions are:

$$\frac{d^2u_{12}}{dy^2}-\left(i\omega R_1+M_1{}^2\right)\left(1+\lambda_1\right)u_{12}+R_1\left(1+\lambda_1\right)P_o=0 \tag{26}$$

$$\frac{d^2u_{22}}{dy^2}+C_p\frac{dc_o}{dy}-\left(i\omega R_2+M_2{}^2\right)u_{22}+\rho R_2P_o=0$$
$$\frac{d^2c_o}{dy^2}-n\frac{du_{22}}{dy}-\left(2n+i\omega R_2P_j\right)c_o=0 \tag{27}$$

$$\frac{d^2u_{32}}{dy^2}-\left(i\omega R_3+M_3{}^2\right)\left(1+\lambda_2\right)u_{32}+\rho' R_1\left(1+\lambda_2\right)P_o=0 \tag{28}$$

$$\frac{\partial u_{12}}{\partial y}=\alpha\sigma_1\left(u_{12}{}'-\frac{R_1}{\sigma_1{}^2}P_o\right),\ u_{12}{}'=u_{12}\qquad \text{at}\quad y=-1 \tag{29}$$

$$\frac{\mu}{m\left(1+\lambda_1\right)}\frac{\partial u_{12}}{\partial y}=\frac{1}{C_p}\frac{\partial u_{22}}{\partial y}+c_o,\ c_o=0,\ u_{12}=u_{22}\qquad \text{at}\quad y=0 \tag{30}$$

$$\frac{\mu'}{m\left(1+\lambda_2\right)}\frac{\partial u_{32}}{\partial y}=\frac{1}{C_p}\frac{\partial u_{22}}{\partial y}+c_o,\ c_o=0,\ u_{22}=u_{32}\qquad \text{at}\quad y=\delta_1 \tag{31}$$

$$\frac{\partial u_{32}}{\partial y}=-\alpha\sigma_2\left(u_{32}{}'-\rho'\frac{R_3}{\sigma_2{}^2}P_o\right),\ u_{32}{}'=u_{32}\qquad \text{at}\quad y=2 \tag{32}$$

2.2 The solution of the problem

The pulsatile velocity field is expressed (33-36)

$u_1=u_{11}+u_{12}e^{i\omega t},\ u_2=u_{21}+u_{22}e^{i\omega t},\ c=c_s+c_oe^{i\omega t},\ u_3=u_{31}+u_{32}e^{i\omega t}.$

The instantaneous mass flux is

$$Q=\int_{-1}^{0}u_1dy+\int_{0}^{1}u_2dy+\int_{1}^{2}u_3dy \tag{37}$$

The shear stress at both the permeable beds is given by

$$\tau=\frac{1}{(1+\lambda)R_1}\frac{\partial u}{\partial y}\Big|_{y=-1,2} \tag{38}$$

3. Results and Discussions

The present section of the work examines the influence of various parameters on the dimensionless representation of the overall and unsteady velocity, microrotation velocity, and mass flux. Our investigation focuses on examining the impact of Reynolds number, Hartmann number, coupling, micropolar, permeability, slip, Jeffrey, and frequency parameters on the flow variables shown in Figures (2-6) for $(\rho=1,\ \rho'=1.4,\ \mu=1.2,\ \mu'=0.8,$ $P_s=1,\ P_o=1,\ \sigma_1=\sigma_2=\sigma=5,\ R_2=\frac{\mu}{\rho}R_1,\ R_3=\frac{\mu}{\rho',\mu'}R_1)$. Further, the results of stress distribution at the top and bottom permeable beds are shown in the table.

Figure 2 depicts the changes in pulsating over time (t). At the interfaces of the bottom $(y=-1)$ and top $(y=2)$ permeable beds, the slip velocities are represented by the velocity. By assigning the values $(\sigma=5,\ M=1,$ $\delta_1=1,\ C_P=1,\ \lambda_1=\lambda_2=\lambda=0.2,\ m=0.5,\ \omega=1,\ R_1=0.5,\ P_j=1,\ n=0.5)$ in which relevant parameters vary while keeping the other parameters constant.

Figure 3 displays the velocity $u(y,t)$ distribution for different parameters. By assigning the values $(\sigma=5,$ $C_P=1,\ M=1,\ \lambda_1=\lambda_2=\lambda=0.2,\ m=0.5,\ \delta_1=1,\ \omega t=\pi/4,\ P_j=1,\ R_1=0.5,\ n=0.5)$ in which relevant parameters vary while keeping the other parameters constant. Figure 3.a) illustrates that the velocity $u(y,t)$ drops as the Coupling parameter rises, indicating stronger micro-rotational interactions that resist fluid motion.

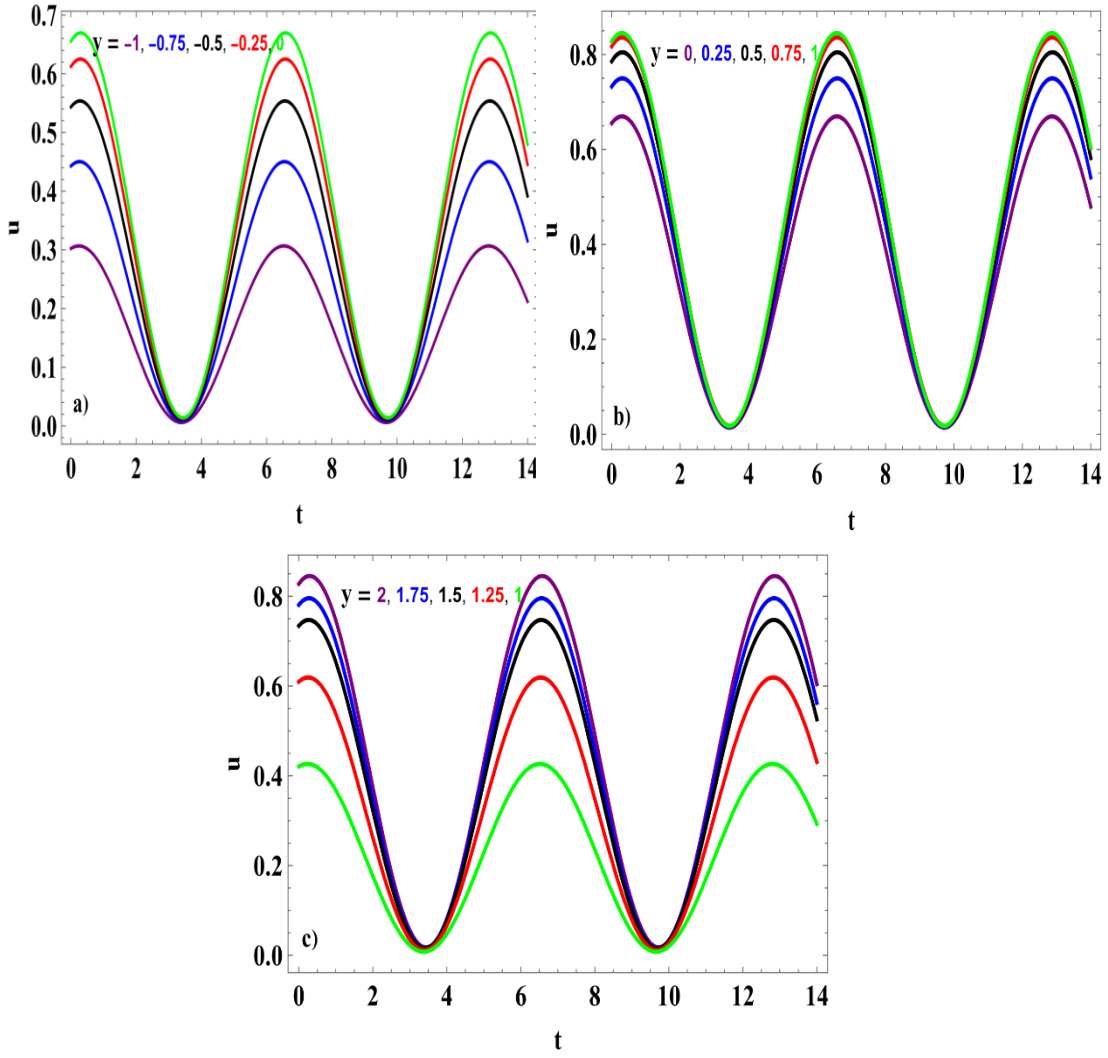

Fig. 2: Velocity distribution for a) Region-A, b) Region-B, c) Region-C

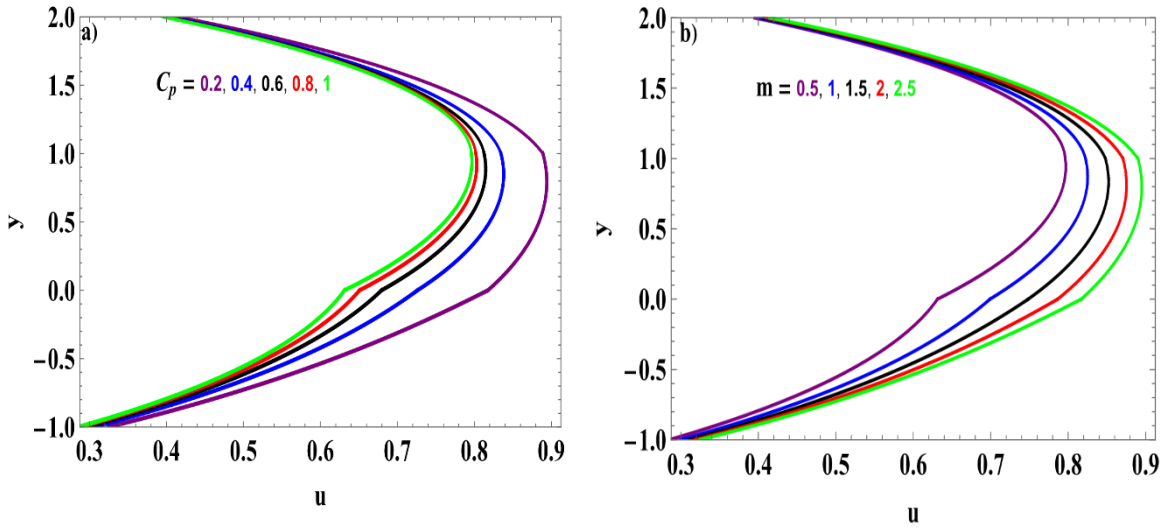

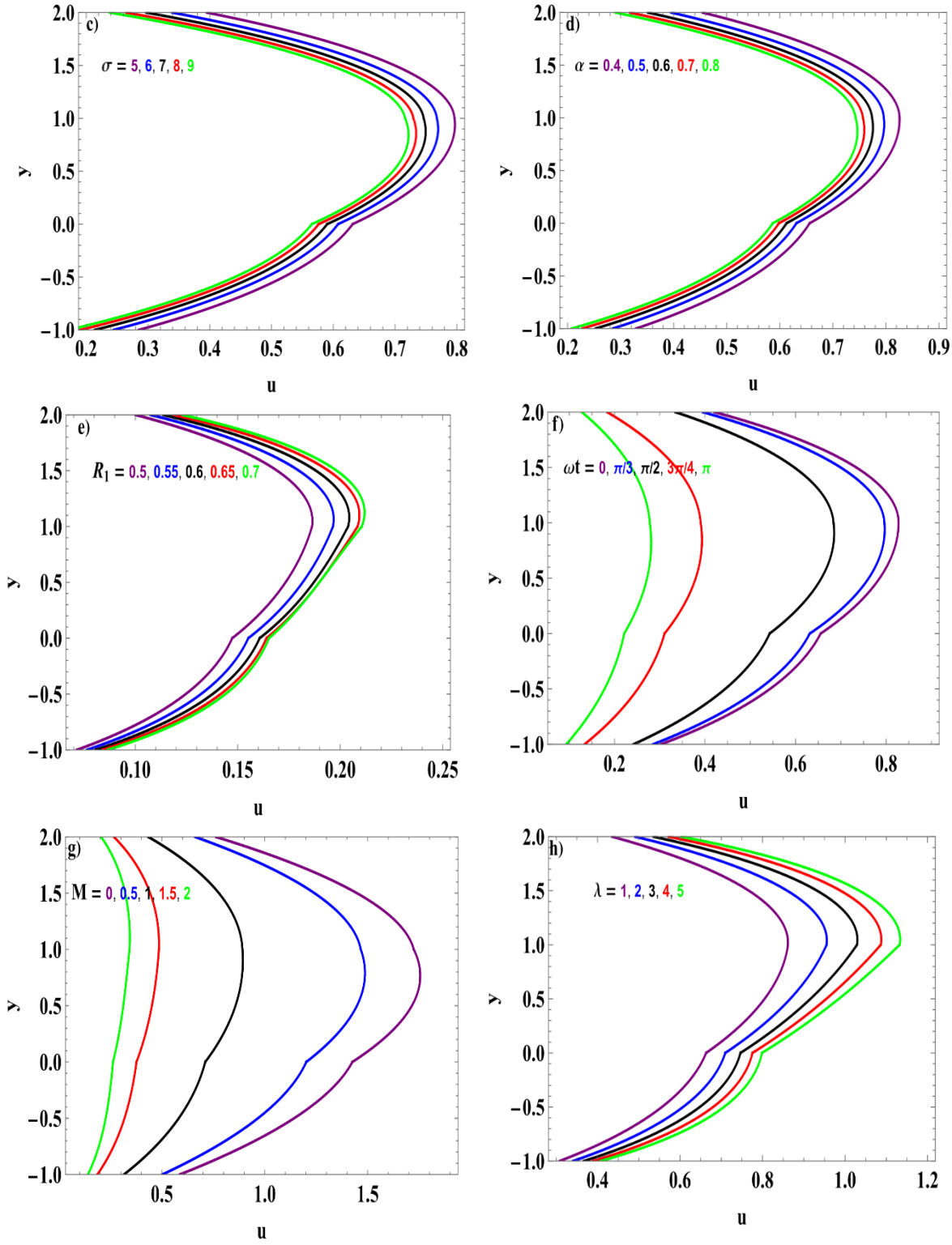

Fig. 3: Velocity distribution for different values of a) C_p, b) m, c) σ, d) α, e) R_1, f) ωt, g) M and λ

In Figure 3.b), the impact of micropolar fluid material parameter on the velocity is depicted. As the value of this parameter grows, a corresponding increase in the velocity $u(y,t)$ observed. The effect of the Porosity parameter on velocity shows in Figure 3.c). As the Porosity parameter increases, it is seen that velocity falls. In Figure 3.d),

the velocity $u(y,t)$ falls as the Slip parameter boost. Figure 3.e) indicates the velocity $u(y,t)$ enhances with the increasing Reynolds number. Figure 3.f) illustrates that the velocity $u(y,t)$ minimize as the Frequency parameter grows. Figure 3.g) shows that the velocity $u(y,t)$ decreases when the Hartmann number increases. Figure 3.h) shows that the velocity $u(y,t)$ of the liquid enhances with the rise of the Jeffrey fluid parameter, which lowers fluid resistance by adjusting fluid elasticity.

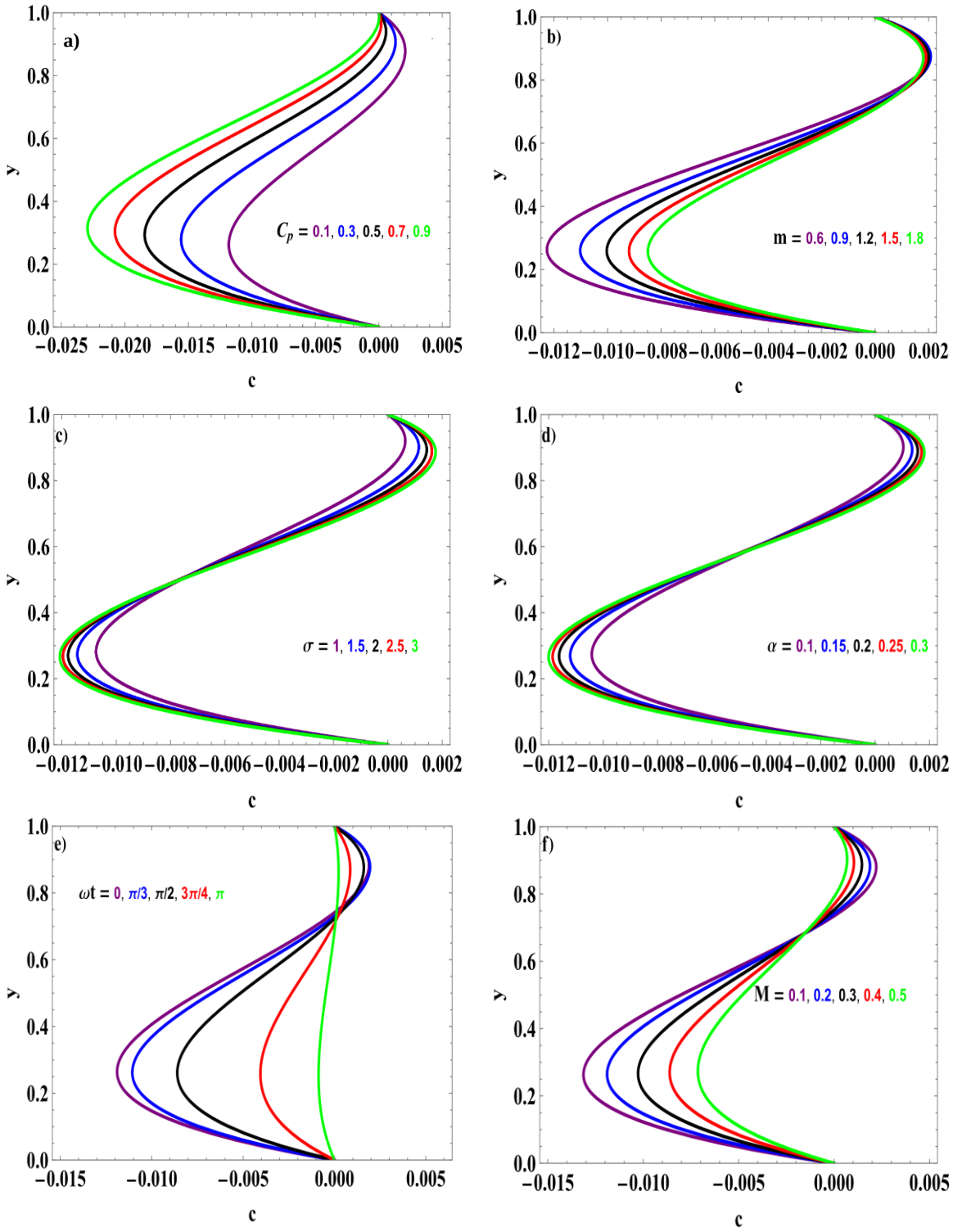

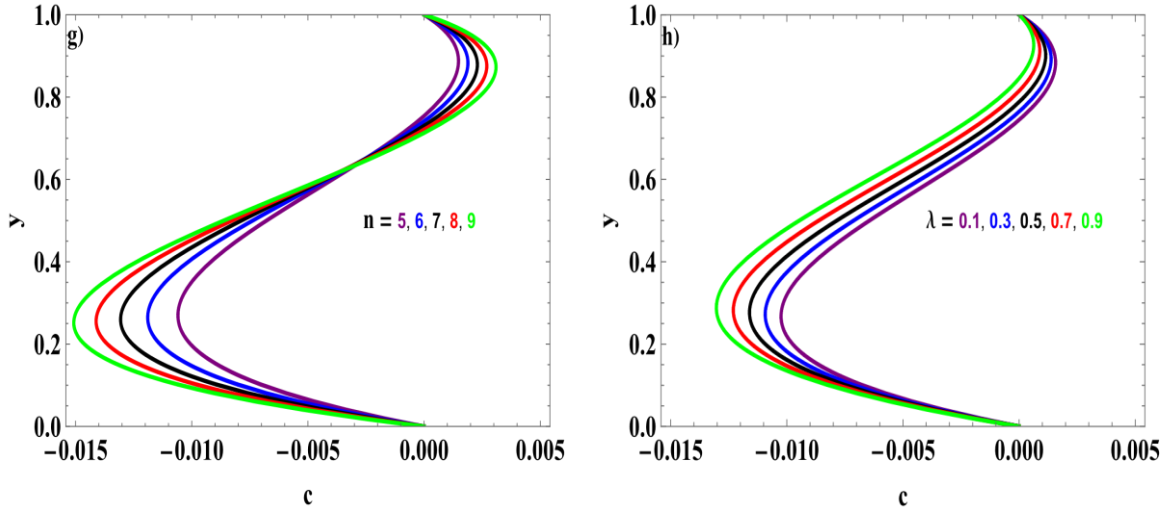

Fig. 4: microrotation Variation with Various parameters.

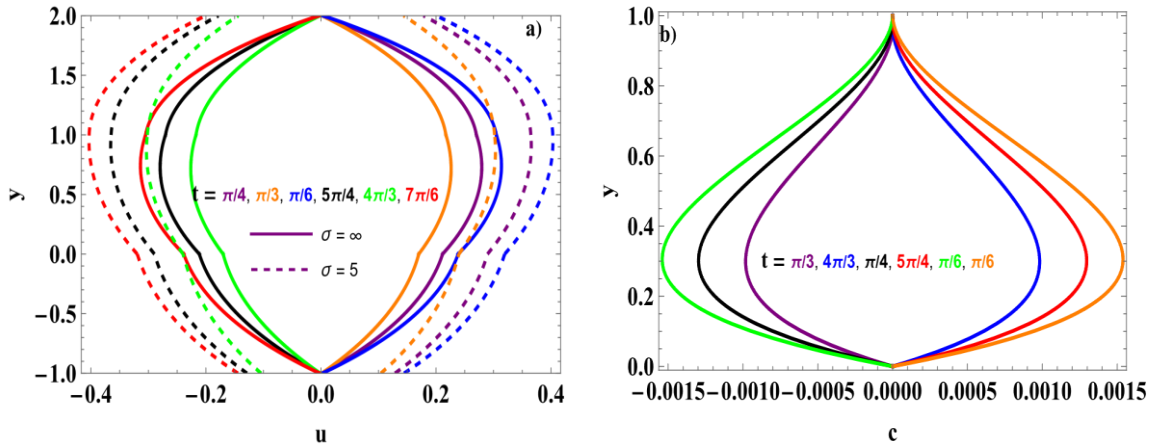

Fig. 5: Unsteady velocity and microrotation

Figure 4 shows the changes in microrotation $c(y,t)$ in core region(Region-B) with various parameters for $(M=0.2,\ C_P=1,\ \lambda_1=\lambda_2=\lambda=0.2,\ \omega t=\pi/6,\ \delta_1=1,\ m=0.6,\ \omega=1,\ P_j=1,\ R_1=0.1,\ n=6)$ in which relevant parameters varying while keeping the other parameters constant.

Figure 4.a) illustrates that the microrotation velocity exhibits a decreasing trend in the central region with the rise in the coupling parameter. Figure 4.b) exhibits in the central core region of the channel $y=0$ to $y=1$, the microrotation velocity falls near the upper interface of the region (R-B) where Jeffrey liquid flows and enhances closer the lower interface with the rise of and Micropolar fluid material parameters. Figure 4.c) shows as the porosity parameter rises, the microrotation velocity in the middle region shows an increasing trend closer to the upper interface $(y=1)$ and a decreasing trend at the lower interface $(y=0)$. Figure 4.d) depicts as the slip parameter grows, the microrotation in the middle region shows a declining pattern near the lower interface $(y=0)$ and a rising trend closer to the higher interface $(y=1)$. Figure 4.e) indicates that as the frequency parameter rises the microrotation velocity in the channel's central core location $y=0$ to $y=1$ falls near the top interface and enhances near the bottom interface of the Region-B. Figure 4.f) demonstrates that in the central core region of the channel $y=0$ to $y=1$, the microrotation velocity declines near the interface $(y=1)$ and rises closer to the lower interface of region-B as the Hartmann number rises. Figure 4.g) displays that the microrotation, denoted as $c(y,t)$, increases near the upper interface $(y=1)$ and reduces closer to the bottom interface $(y=0)$ when the gyration parameter increases. Figure 4.h) exhibits that the microrotation $c(y,t)$ decreases in the Region-B when the Jeffrey fluid material parameter increases Figure 5 illustrates the unsteady velocity and microrotation.

Figure 5.a) depicts that the unsteady velocity fluctuates over time with or without permeability. Similarly, the unsteady microrotation velocity fluctuates over time, which can be observed in Figure 5.b).

Table 1: Shear stress variation with several variables.

ωt		$\alpha \to 0.1$	0.2	0.3	0.4	0.5	$\sigma \to 1$	3	5	7	9
0	LPB	1.46319	1.77089	1.90185	1.97397	2.01953	1.17579	1.87566	2.01953	2.08137	2.11574
	UPB	1.38797	1.73075	1.88845	1.97944	2.03873	0.97145	1.84507	2.03873	2.12501	2.17397
$\pi/4$	LPB	1.29179	1.63022	1.77525	1.85348	1.90182	1.07389	1.75543	1.90182	1.96317	1.99653
	UPB	1.26476	1.62685	1.79362	1.88807	1.94852	0.92109	1.75786	1.94852	2.03173	2.07817
$\pi/2$	LPB	1.07499	1.36776	1.49702	1.56638	1.60836	1.07389	1.75543	1.90182	1.96317	1.99653
	UPB	1.11653	1.43917	1.58989	1.67433	1.72725	0.92109	1.75786	1.94852	2.03173	2.07817
$3\pi/4$	LPB	0.87761	1.08030	1.16104	1.20009	1.22119	0.98699	1.18437	1.22119	1.23094	1.23343
	UPB	0.98917	1.24435	1.35576	1.41433	1.44871	0.95080	1.36459	1.44871	1.47884	1.49248
ωt		$R_1 \to 0.5$	1	1.5	2	2.5	$m \to 0.1$	0.2	0.3	0.4	0.5
0	LPB	2.01953	1.97397	1.90185	1.77089	1.46319	1.73876	1.81731	1.88916	1.95619	2.01953
	UPB	2.03873	2.76215	3.48557	4.20899	4.93242	1.93033	1.95176	1.97825	2.00765	2.03873
$\pi/4$	LPB	1.29179	1.63022	1.77525	1.85348	1.90182	1.07389	1.75543	1.90182	1.96317	1.99653
	UPB	1.26476	1.62685	1.79362	1.88807	1.94852	0.92109	1.75786	1.94852	2.03173	2.07817
$\pi/2$	LPB	1.90182	1.79138	1.66251	1.55721	1.47679	1.64801	1.71947	1.78465	1.84511	1.90182
	UPB	1.94852	2.39998	2.61732	2.72099	2.77901	1.84846	1.86877	1.89313	1.92028	1.94852
$3\pi/4$	LPB	0.87761	1.08030	1.16104	1.20009	1.22119	0.98699	1.18437	1.22119	1.23094	1.23343
	UPB	0.98917	1.24435	1.35576	1.41433	1.44871	0.95080	1.36459	1.44871	1.47884	1.49248
ωt		$n \to 0.5$	1	1.5	2	2.5	$P_j \to 1$	5	10	15	20
0	LPB	2.01952	2.01737	2.01546	2.01376	2.01224	2.01952	2.01956	2.01961	2.01965	2.01969
	UPB	2.03873	2.04108	2.04316	2.04501	2.04667	2.03873	2.03867	2.03861	2.03855	2.03849
$\pi/4$	LPB	1.29179	1.63022	1.77525	1.85348	1.90182	1.07389	1.75543	1.90182	1.96317	1.99653
	UPB	1.26476	1.62685	1.79362	1.88807	1.94852	0.92109	1.75786	1.94852	2.03173	2.07817
$\pi/2$	LPB	1.90182	1.89981	1.89804	1.89646	1.89503	1.90182	1.90191	1.90207	1.90225	1.90239
	UPB	1.94851	1.95067	1.95209	1.95428	1.95580	1.94852	1.94843	1.94829	1.94816	1.94805
$3\pi/4$	LPB	0.87761	1.08030	1.16104	1.20009	1.22119	0.98699	1.18437	1.22119	1.23094	1.23343
	UPB	0.98917	1.24435	1.35576	1.41433	1.44871	0.95080	1.36459	1.44871	1.47884	1.49248
ωt		$C_P \to 0.2$	0.4	0.6	0.8	1.0	$\lambda \to 0.1$	0.2	0.3	0.4	0.5
0	LPB	2.93641	2.42406	2.21254	2.09507	2.01953	2.01952	1.93757	1.86898	1.81025	1.75900
	UPB	2.63166	2.27878	2.14566	2.07829	2.03873	2.03873	2.03811	2.04437	2.05543	2.06989
$\pi/4$	LPB	1.29179	1.63022	1.77525	1.85348	1.90182	1.07389	1.75543	1.90182	1.96317	1.99653
	UPB	1.26476	1.62685	1.79362	1.88807	1.94852	0.92109	1.75786	1.94852	2.03173	2.07817
$\pi/2$	LPB	2.65709	2.25129	2.07156	1.96886	1.90182	1.90182	1.82272	1.75611	1.69875	1.64839
	UPB	2.45345	2.16021	2.04411	1.98413	1.94852	1.94852	1.94147	1.94046	1.94341	1.94892
$3\pi/4$	LPB	0.87761	1.08030	1.16104	1.20009	1.22119	0.98699	1.18437	1.22119	1.23094	1.23343
	UPB	0.98917	1.24435	1.35576	1.41433	1.44871	0.95080	1.36459	1.44871	1.47884	1.49248

Table 1 shows the variation of the shear stress τ at both permeable beds with slip, porosity, Reynolds, micropolar material, gyration, microrotation, coupling, Jeffrey fluid, and Hartmann parameters by assigning values for $(\rho=1,\ \rho'=1,\ \lambda_1=\lambda_2=\lambda=0.1,\ \mu=1.2,\ \mu'=0.8,\ P_j=1,\ \delta_1=1,\ P_s=1,\ P_o=1,\ \sigma=5,\ M=0.5,\ C_P=1,$ $n=0.5,\ m=0.5,\ R_1=0.5,\ R_2=\frac{\mu}{\rho}R_1,\ R_3=\frac{\mu}{\rho',\mu'}R_1)$ in which relevant parameters vary while keeping the other parameters constant.

As the slip and porosity parameters increase, there is a noticeable rise in stress distribution at both the lower and upper permeable beds. In contrast, an increase in the Reynolds number, micropolar material, and gyration parameters results in a reduction of shear stress at the LPB, while simultaneously enhancing it at the UPB. When the microrotation parameter increases, shear stress at the LPB rises, but it shows revers trend at the UPB. Furthermore, with the rise of coupling and Jeffrey fluid parameters, there is a decline in shear stress at both beds.

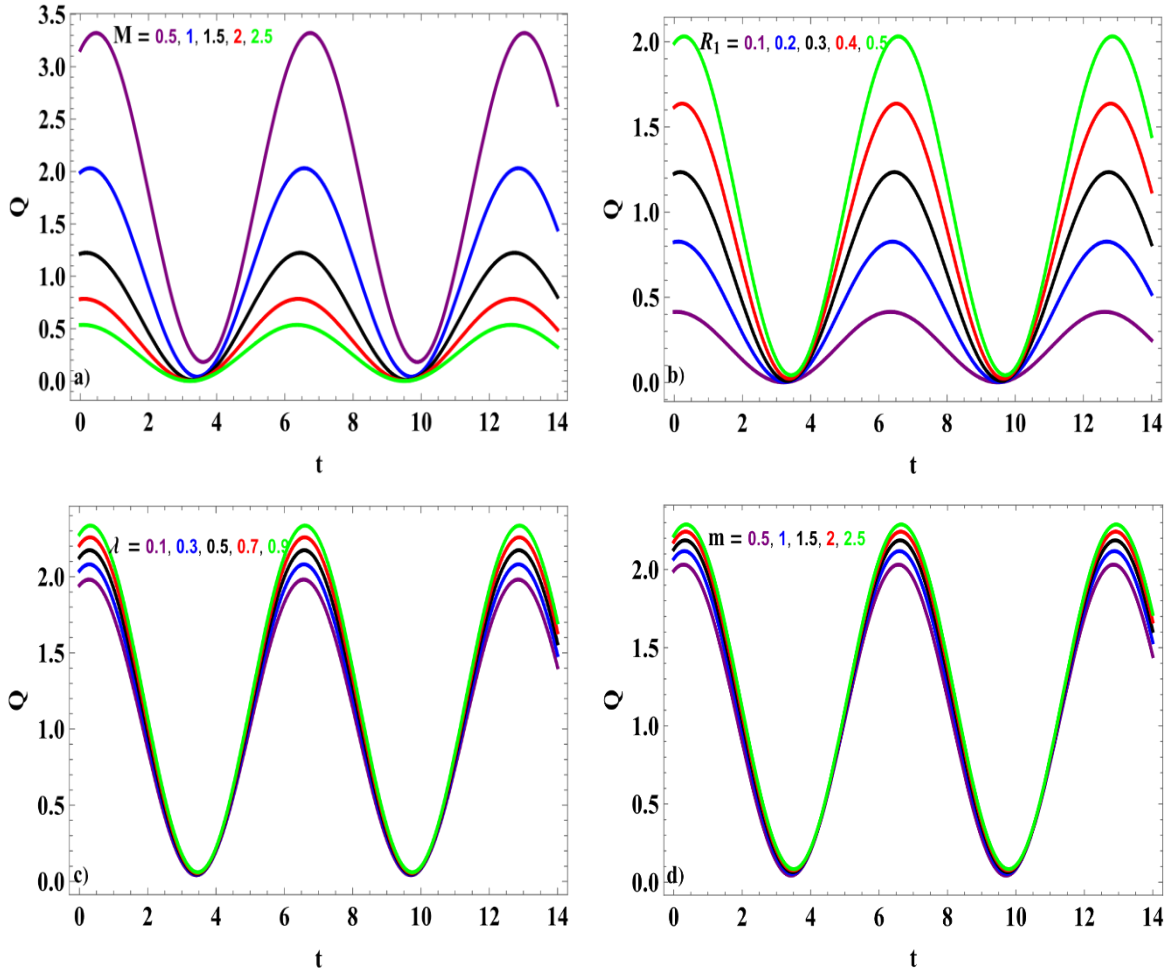

Fig. 6: Mass flux variation with several parameters.

Figure 6 represents the variation in mass flux variation with different parameters for ($\lambda_1 = \lambda_2 = \lambda = 0.2$, $P_j = 1$, $\delta_1 = 1$, $\sigma = 5$, $M = 1$, $C_P = 1$, $n = 0.7$, $m = 0.5$, $R_1 = 0.5$) and keeping the other parameters constant. Figure 6.a) illustra-

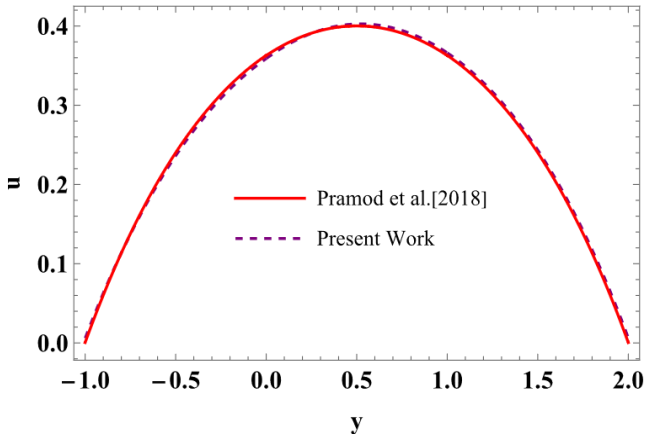

Fig. 7: Comparative study

tes that the mass flux reduces with the rise of the Hartmann number. Figures 6.b), c) and d) demonstrate that the mass flux rises when the Reynolds number, Jeffrey parameter, and micropolar fluid material parameters increase, respectively.

Figure 7 presents a comparative analysis for limiting cases where the permeability and Jeffrey fluid parameters tend to infinity, and the results show excellent agreement with those reported by Pramod et al. (2018).

4. Conclusions

This work investigates the pulsating flow of Jeffrey liquid layers separated by a micropolar liquid layer. The flow occurs between two permeable beds and is influenced by a magnetic field. The Beavers-Joseph slip conditions are applied at the interfaces of the permeable beds. Assuming that the velocity and microrotation velocity comprise steady and oscillatory parts, in view of the periodic pressure gradient, the governing flow equations have been reduced into ordinary differential equations (ODEs). The resulting ODEs are solved numerically using the NDSolve command in Mathematica software. The graphical representations illustrate the impact of different parameters on mass flux, velocity and microrotation velocity. Moreover, the tabulated data on stress distribution at the two permeable beds is provided and analyzed. Here are the findings from the investigation:

- The Hartmann number, slip, porosity, frequency, and coupling parameters all contribute to the suppression of the flow.
- The Reynolds number, Jeffrey parameter, and Micropolar fluid material parameter all escalates the flow.
- The microrotation velocity rises near the upper interface $(i.e.,\ y=1)$ and falls near the lower interface $(i.e.,\ y=0)$ of the central region, influenced by porosity, slip, and gyration parameters.
- In the core region ($y=0$ to $y=1$), the microrotation velocity falls near the upper interface of R-B, where Jeffrey liquid flows and is enhanced closer to the lower interface, driven by the Hartmann number, frequency, and micropolar material parameters.
- Microrotation velocity falls with the rise of Jeffrey and Coupling parameters.
- The unsteady component of velocity and microrotation velocity fluctuates over time.
- At both permeable beds, the shear stress enhances with the rise of Reynolds, Jeffrey, porosity and slip parameters. whereas the stress distribution at both beds falls with a rise in coupling parameter, C_P and Hartman number, M.
- As the gyration parameter increases, at the LPB, the shear stress drops and rises at UPB. On the other hand, when the rise of the microrotation parameter, the stress distribution at the LPB enhances, and diminishes at the UPB.
- The mass flux promotes continuously with the rise of Reynolds number, Jeffrey and Micropolar material parameters, and it falls progressively with the rise of Hartmann number.
- By taking the permeability and Jeffrey parameters to infinity, our analysis shows strong agreement with the findings of other researchers.

CRediT Author Statement

Madhurya Vangalapudi: Mathematical formulation, solution methodology, visualisation, validation, and write-up. **Suripeddi Srinivas:** Problem conceptualisation, model development, and verification.

References

Ali, A., Umar, M., Bukhari, Z., and Abbas, Z. (2020): Pulsating flow of a micropolar-Casson fluid through a constricted channel influenced by a magnetic field and Darcian porous medium: A numerical study. Results in Physics, *19*, 103544. https://doi.org/10.1016/j.rinp.2020.103544

Allan, F. M, Hajji. M. A., and Anwar, M. N. (2009): The characteristics of fluid flow through multilayer porous media. ASME. Journal of Applied Mechanics 76(1): 014501. https://doi.org/10.1115/1.2998483

Beavers, G. S., and Joseph, D. D. (1967): Boundary conditions at a naturally permeable wall. Journal of fluid mechanics, 30(1), 197-207. https://doi.org/10.1017/S0022112067001375

Bhattacharya, D. K., and Nanda, R. S. (1979): On pulsatile flow of a viscous fluid in a rotating channel. Proceedings of the Indian Academy of Sciences-Section A. Part 3, Mathematical Sciences 88 pp.35-48. https://doi.org/10.1007/BF02898333

Bhuvaneswari, M., and Sivasankaran, S. (2024): Double diffusive MHD squeezing copper water nanofluid flow between parallel plates filled with porous medium and chemical reaction. International Journal of Numerical Methods for Heat and Fluid Flow 34.3, 1151-1169. https://doi.org/10.1108/HFF-05-2023-0277

Bitla, P., and Iyengar, T. K. V. K. V. (2013): Pulsating flow of an incompressible micropolar fluid between permeable beds. Nonlinear Analysis: Modelling and Control 18.4, 399-411. https://doi.org/10.15388/NA.18.4.13969

Bitla, P., and Iyengar, T. K. V. (2014): Pulsating flow of an incompressible micropolar fluid between permeable beds with an inclined uniform magnetic field. European Journal of Mechanics-B/Fluids 48, 174-182. https://doi.org/10.1016/j.euromechflu.2014.06.002

Chamkha, A. J., Jawali, C. U., and Mateen, A. (2004): Oscillatory flow and heat transfer in two immiscible fluids. International Journal of Fluid Mechanics Research 31.1. 10.1615/InterJFluidMechRes.v31.i1.20

Chandrapushpam, T., Bhuvaneswari, M., and Sivanandam, S. (2023): Double diffusive MHD squeezing copper water nanofluid flow between parallel plates filled with porous medium and chemical reaction. International Journal of Numerical Methods for Heat and Fluid Flow 34.3, 1151-1169. https://doi.org/10.1108/HFF-05-2023-0277

Chaudhry, M. H. (2014): Applied Hydraulic Transients. Vol. 415. New York: Springer. https://doi.org/10.1007/978-1-4614-8538-4

Eringen, A. C. (1966): Theory of micropolar fluids. Journal of mathematics and Mechanics, Vol. 16, 1-18.

Eringen, A. C. (2001): Microcontinuum field theories: II. Fluent media. Vol. 2. Springer Science and Business Media.

Hakeem, A. A., Priya, S., Bhose, G., and Sivanandam, S. (2024): Magneto-convective hybrid nanofluid slip flow over a moving inclined thin needle in a Darcy-Forchheimer porous medium with viscous dissipation. International Journal of Numerical Methods for Heat and Fluid Flow, 34(1), 334-352. https://doi.org/10.1108/HFF-04-2023-0200

Iyengar, T. K. V., and Bitla, P. (2011): Pulsating flow of an incompressible couple stress fluid between permeable beds. World Academy of Science, Engineering and Technology 56 1355-1365.

Kim, S. Y., Kang, B. H., and Hyun, J. M. (1994). Heat transfer from pulsating flow in a channel filled with porous media. International Journal of Heat and Mass Transfer, 37(14), 2025-2033.https://doi.org/10.1016/0017-9310(94)90304-2

Komal, G., and Srinivas, S. (2024a): Two-layered magnetohydrodynamics of immiscible pulsatile flow in corrugated curved channel. International Journal of Modelling and Simulation pp. 1-19. https://doi.org/10.1080/02286203.2024.2311967

Komal, G., and Srinivas, S. (2024b): Pulsatile flow of Casson hybrid nanofluid between ternary-hybrid nanofluid and nanofluid in an inclined channel with temperature-dependent viscosity. Numerical Heat Transfer, Part A: Applications pp. 1-30. https://doi.org/10.1080/10407782.2024.2314735

Kumar, D., and Agarwal, M. (2021): MHD pulsatile flow and heat transfer of two immiscible couple stress fluids between permeable beds. Kyungpook Mathematical Journal, 61(2), 323-351. https://doi.org/10.5666/KMJ.2021.61.2.323

Malathy, T., and Srinivas, S. (2008): Pulsating flow of a hydromagnetic fluid between permeable beds. International Communications in Heat and Mass Transfer 35.5 pp. 681-688. https://doi.org/10.1016/j.icheatmasstransfer.2007.12.006

Mukherjee, S., and Shit, G. C. (2022): Mathematical modeling of electrothermal couple stress nanofluid flow and entropy in a porous microchannel under injection process. Applied Mathematics and Computation, 426, 127110. https://doi.org/10.1016/j.amc.2022.127110

Okedoye, A. M. (2025): Heat transfer in hydromagnetic oscillatory flow past an impulsively started porous limiting surface. Journal of Naval Architecture and Marine Engineering, 22(2), 183–197. https://doi.org/10.3329/jname.v22i2.32114

Padma, D. M. and Srinivas, S. (2023): Two layered immiscible flow of viscoelastic liquid in a vertical porous channel with Hall current, thermal radiation and chemical reaction. International Communications in Heat and Mass Transfer, 142, 106612. https://doi.org/10.1016/j.icheatmasstransfer.2023.106612

Padma, D. M., Srinivas, S., and Vajravelu, K. (2024): Entropy generation in two-immiscible MHD flow of pulsating Casson fluid in a vertical porous space with Slip effects. Journal of Thermal Analysis and Calorimetry, 149(14). https://doi.org/10.1007/s10973-024-13337-8

Rajkumar, D., Subramanyam Reddy, A., and Chamkha, A. J. (2025): Entropy generation of magnetohydrodynamic pulsating flow of micropolar nanofluid in a porous channel through Cattaneo–Christov heat flux model with Brownian motion, thermophoresis and heat source/sink. Waves in Random and Complex Media, 35(6), 11763-11788. https://doi.org/10.1080/17455030.2022.2124467

Sankar, D. S., and Lee, U. (2009): Mathematical modeling of pulsatile flow of non-Newtonian fluid in stenosed arteries. Communications in Nonlinear Science and Numerical Simulation, 14(7), 2971-2981. https://doi.org/10.1016/j.cnsns.2008.10.015

Selvi, R. K., and Muthuraj, R. (2018): MHD oscillatory flow of a Jeffrey fluid in a vertical porous channel with viscous dissipation. Ain Shams Engineering Journal 9.4 pp. 2503-2516. https://doi.org/10.1016/j.asej.2017.05.009

Sivanandam, S., and Alqurashi, T. J. (2025). Activation energy and cross-diffusion effects on 3D rotating nanofluid flow in a Darcy–Forchheimer porous medium with radiation and convective heating. Open Physics, 23(1), 20250186. 10.1515/phys-2025-0186

Umavathi, J. C., Chamkha, A. J., and Shekar, M. (2014): Flow and heat transfer of two micropolar fluids separated by a viscous fluid layer. International Journal of Microscale and Nanoscale Thermal and Fluid Transport Phenomena, 5(1), 23. https://doi.org/10.1108/HFF-09-2015-0354

Umavathi J. C., and Hemavathi, K. (2018): Heat transfer of nanofluid sandwiched between regular fluid. Journal of Nanofluids 7.3, pp. 536-543. https://doi.org/10.1166/jon.2018.1476

Vajravelu, K., Arunachalam, P. V., and Sreenadh, S. (1995): Unsteady flow of two immiscible conducting fluids between two permeable beds. Journal of mathematical analysis and applications, 196(3), 1105-1116. https://doi.org/10.1006/jmaa.1995.1463

Valueva, E. P., and Purdin, M. S. (2015): The pulsating laminar flow in a rectangular channel. Thermophysics and Aeromechanics, 22(6), 733-744. https://doi.org/10.1134/S0869864315060098

Wang, Y.C. (1971): Pulsatile flow in a porous channel, Trans ASME, Journal of Applied Mechanics, 38, pp.553–555. https://doi.org/10.1115/1.3408822

Zamir, M., and Budwig, R. S. (2002): Physics of pulsatile flow. Applied Mechanics Reviews, 55(2), B35-B35. https://doi.org/10.1115/1.1451229.